*J. Fluid Mech.* (1994), *vol.* 267, *pp.* 353–376



# The flapping shear layer formed by flow separation from the forward corner of a square cylinder

By D. A. LYN[1] AND W. RODI[2]

[1] School of Civil Engineering, Purdue University, W. Lafayette, IN 47907, USA

[2] Institute for Hydrodynamics, University of Karlsruhe, D-7500 Karlsruhe, Germany

(Received 22 May 1992 and in revised form 19 November 1993)

The turbulent shear layer and the associated recirculation region on the sidewall formed in flow separation from the forward corner of a square cylinder have been studied with one-component laser-Doppler velocimetry. Because of vortex shedding, the flow is approximately periodic, and is treated as a separated flow undergoing large-amplitude forcing at the shedding frequency. Phase (ensemble)-averaged velocities and turbulence intensities were obtained, and a close relationship in phase and amplitude between phase-averaged turbulence intensities and gradients of phase-averaged velocity is found in much of the flow region. The similarity behaviour of the phase-averaged profiles in the shear layer as well as the streamwise growth of the shear layer are investigated. While phase-averaged velocity profiles collapse well in similarity coordinates, normalized turbulence intensities exhibit systematic deviations from similarity. Shear-layer growth also departs markedly from the linear growth law of unforced plane mixing layers. The effect of the recirculation is suggested as a possible explanation for some of these deviations. Similarities to and differences from steady and forced mixing layers, steady separated flows with recirculation, and unsteady boundary layers are discussed.

## 1. Introduction

### 1.1. *Scope and motivation*

Unsteady turbulent flows have received increasing attention from researchers, motivated in part from the importance of unsteadiness in industrial problems arising in turbomachinery and aeronautics. Periodic excitation of a basic steady turbulent flow has also provided insights into turbulence structure, since this may highlight events involving large-scale structures, which would otherwise be overlaid with a large amount of noise. Flows with externally imposed time-varying disturbances, such as a periodic free-stream velocity or external pressure gradient above a boundary layer (Simpson, Shivaprasad & Chew 1983), or a plane mixing layer forced by an oscillating flap along the edge of the splitter plate (Oster & Wygnanski 1982; Weisbrot & Wygnanski 1988) lend themselves more easily to analysis since the underlying temporal variation is known. Naturally occurring flows with pronounced periodic features present a more difficult experimental problem, since a fixed unambiguous reference time variation is not available. A procedure for determining a reference must be developed, and since, even if the natural flow is strongly periodic, it is narrow-banded rather than monochromatic, such a procedure necessarily involves greater measurement uncertainty.

The turbulent separated flow around two-dimensional bluff bodies exhibits a self-

induced quasi-periodicity due to vortices being 'shed' alternately from either side of the body. The near-field wake flow behind the bluff body is not only temporally but also spatially extremely complex, with direct interaction between the two separated shear layers and regions of irrotational flow entrained into the wake. The present work reports on the first part of a larger experimental and numerical study of various aspects of the flow around square cylinders. It presents ensemble-averaged (averages at constant phase, or more briefly phase-averaged) one-component velocity measurements obtained with a laser-Doppler system in the flow region between the free stream and a cylinder sidewall, including the separated shear layer but preceding any direct interaction between shear layers. Two-component measurements in the near-wake region further downstream have been completed and will be presented in a subsequent paper. The focus on the unsteady 'flapping' single shear layer very close to the body avoids much of the spatial complexity of the near-wake flow, and may also provide some insight into the unsteady features observed in nominally steady separated flows, e.g. the flow around a bluff plate (Kiya & Sasaki 1983; Cherry, Hillier & Hillier 1984; Djilali & Gartshore 1991). It may also be relevant to practical problems in heat and mass transfer from bluff bodies, where near-wall effects are expected to be dominant. Previous related studies with ensemble-averaged statistics, e.g. the study of the turbulent flow around a single circular cylinder of Cantwell & Coles (1983), have been concerned primarily with the flow behind the body. Studies of the steady separated flows, on the other hand, have been mostly restricted to time-averaged statistics, although conditional sampling (e.g. Kiya & Sasaki 1983) and spatial correlations (Cherry *et al.* 1984) have been used.

The experimental distinction between organized and random variations in time is crucial to ensemble averaging when the underlying time variation is not known *a priori*. Studies of the ensemble-averaged near-field flow around single circular cylinders (Owen & Johnson 1980; Cantwell & Coles 1983) based their reference signal on a probe (pressure sensor or surface hot-film sensor) located at the surface of a cylinder sidewall. Perry & Steiner (1987) in a similar study of a plate oblique (including normal) to the incident flow defined phase according to a fixed hot-wire probe in the non-turbulent part of the flow just outside of the wake. Hussain (1986) has discussed 'education' schemes for detecting structure in turbulent flows, and notes two sources of phase jitter, namely that due to randomness in the initiation of a structure and that due to randomness in their evolution. Schemes using a single fixed sensor are aimed at reducing the former but may still be susceptible to the latter. In this work, the phase reference is based on a single pressure sensor located in the centre of a cylinder sidewall. Because of the rather restricted flow region considered, 'evolution' jitter should be minimal.

With a meaningful phase definition, the instantaneous value of a flow variable, $f(t)$, may be decomposed into a phase-varying or periodic component, $\langle f \rangle$, and a 'random' component, $f'$. A further decomposition of $\langle f \rangle$ into a time-averaged mean component, $\bar{f}$, and a periodic component with zero mean, $\tilde{f}$, results in the triple decomposition (Hussain & Reynolds 1970):

$$f(t) = \langle f \rangle + f' = \bar{f} + \tilde{f} + f'. \tag{1}$$

In treating the unsteady aspects of flow around a square cylinder in a simplified manner, Durao, Heitor & Pereira (1988) band-reject filtered the velocity time series at each measuring point to remove the dominant frequency contribution due to vortex shedding. The residual was then treated as a conventional turbulent signal, where long-time averaging could possibly be justified. A somewhat similar procedure is based on

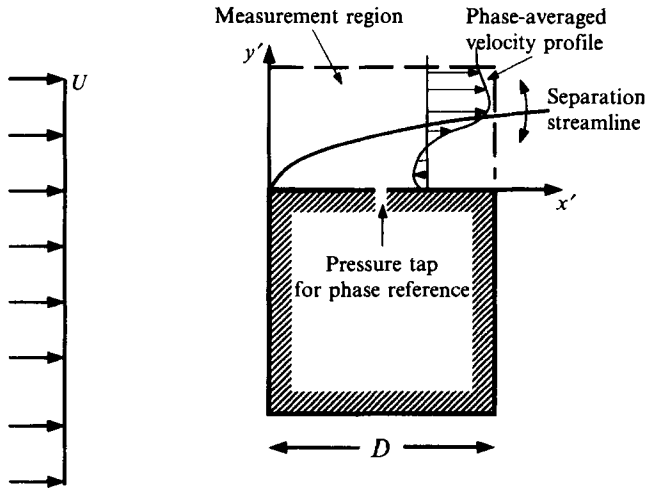


FIGURE 1. Definition sketch of a flapping shear layer, formed by flow separation from the forward corner of a square two-dimensional cylinder.

spectral estimates, i.e. subtracting the periodic contribution from the total energy, and defining the residual broad-band contribution as the stochastic part (Gaster, Kit & Wygnanski 1985; Fiedler & Mensing 1985). This average overall turbulence intensity excluding the periodic contribution may be considered in the context of the triple decomposition as the average over all phases of the phase-averaged turbulence intensity, denoted here as $u'_0$, and should be distinguished from the time-averaged turbulence intensity, denoted as $\overline{u'}$. The distinction between coherent and random variations, based on an assumption of a wide separation of timescales, remains somewhat artificial and the 'random' fluctuations are best viewed as a residual. The approach is akin to the traditional Reynolds-averaging in this regard, except that the averaging is performed over a given ensemble or phase bin rather than over the entire record length. The evident large-scale periodic structure is resolved, but finer-scale features which may or may not exhibit some 'structure' are classified as being statistically stationary turbulence, which can be described usefully by statistical measures, and perhaps be modelled more easily. In particular, the high-frequency small-scale phenomena associated with the fundamental instability of the shear layer is *not* resolved. Such an approach is similar to that taken in large-eddy (or very large-eddy) simulations.

The square cylinder was chosen as a simple, compactly characterized bluff body, the separation point(s) of which are fixed and known, unlike the case of the circular cylinder, where the separation points are known to wander in time. A further advantage of this geometry, noted by workers in steady-flow cases (Kiya & Sasaki 1983; Cherry *et al.* 1984), is the highly favourable pressure gradient just prior to separation, which results in an extremely thin separating shear layer; effects on shear-layer development due to the initial shear-layer thickness should therefore be negligible. The square geometry also has an advantage in numerical modelling, and therefore, turbulence model verification, and shares some geometrical similarities with the rectangular bluff-plate flow that has been frequently studied. The flow region studied and the coordinate system used later in the presentation of results are shown in figure 1. The origin is taken at the point of separation at one of the upstream edges of the cylinder.

Preliminary flow visualization indicated that the initial separated shear layer was laminar, with transition occurring soon after separation. In their study of a bluff-plate flow at a comparable Reynolds number, $Re = UD/\nu$ ($\nu$ is the kinematic viscosity of the fluid), Cherry *et al.* (1984) also observed laminar separation, and estimated that transition was completed within $0.3D$ of separation. Since most of the measurements were made in the region beyond this distance, the present study considers the flow as being essentially fully turbulent. The flow is treated as an unsteady separated shear flow bounding a recirculation region under large-amplitude forcing at the vortex shedding frequency, $f_s$. The broad question addressed concerns the extent to which the unsteady turbulent flow in the immediate vicinity of the cylinder, resulting from separation at a cylinder corner, resembles other simple steady or unsteady turbulent flows, e.g. the nominally steady flow around a bluff plate, or the forced mixing layer. In particular, are general classical concepts such as gradient transport or self-similarity still relevant or useful in characterizing the basic features of such a 'flapping' shear layer bounding a recirculation region?

## 2. Experimental equipment and conditions

### 2.1. *Flow parameters*

Measurements were made in a closed water channel with a working cross-section of 56 cm × 39 cm. The square aluminium cylinder was of diameter $D = 4$ cm, and length $L = 39$ cm, resulting in a blockage of 7% and an aspect ratio of 9.75. Circular taps, 1 mm in diameter, were bored in the cylinder at midheight and at the midpoint between corners to be used for the pressure signal used for phase definition. At the farthest accessible upstream point, $\approx 2.5D$ in front of the cylinder, the velocity profile was found to be still affected by the presence of the cylinder, with a centreline defect of 5%–10% compared to the free stream. Durao *et al.* (1988) under slightly different conditions (blockage of 14%, aspect ratio of 6, and Reynolds number of 14000) reported negligible upstream effects for distances $2D$ from a square cylinder. From the inlet profile, the averaged approach velocity $U = 0.535$ m s$^{-1}$, giving $Re = 21400$. At the streamwise location of the cylinder, because of blockage, the free-stream velocity was 0.59 m s$^{-1}$. The level of free-stream turbulence, $\overline{u'}/U$ (the bar indicates a time-averaged quantity), measured upstream of the cylinder was found to be $\approx 2\%$ (this was also the level in the absence of the cylinder). The vortex shedding frequency, $f_s$, was determined to be $1.79 \pm 0.05$ Hz, from direct as well as spectral analysis of the low-pass-filtered pressure signal. The Strouhal number, $St = f_s D/U = 0.134$, agrees with values reported in the literature for square cylinders (Okajima 1982; Durao *et al.* 1988). In the following, unless otherwise specified, velocity quantities are normalized by $U$, and lengths or distances are normalized by $D$.

### 2.2. *The laser-Doppler (LDV) system*

Velocity measurements were obtained with a laser-Doppler system. In much of the region of study, only one-component measurements could be obtained using the available laser-Doppler system because of restricted optical accessibility. A two-component, four-beam system, with one pair of beams being masked, was operated in the forward-scatter on-axis-collection real-fringe mode. A Bragg cell unit was used to produce frequency shifts in the range 100–200 kHz. The minor axis of the probe volume was estimated to be $\approx 0.3$ mm, while the major axis was estimated to be 5 mm in length. The photomultiplier signal was band-pass filtered and amplified before being

digitized at 10 MHz (compared to maximum signal frequencies of 0.4 MHz) by a Vuko VKS 220-16 transient recorder. A software validation step using a zero-crossing counting algorithm with symmetric noise thresholds (essentially emulating a counter processor) was performed, and the Doppler shift frequency of the validated signal was then determined. The closest measurement points were generally located 3 mm from the wall. This was insufficient to resolve the wall layer, i.e. the region below the point at which the maximum negative velocity was found, for all phases. The accuracy in defining the distance from the wall is believed to be $\pm 0.4$ mm. Measurements were taken at eight sections, from $x = 0$ to $x = 1$, at equally spaced intervals of $\Delta x = 0.125$, except for the section at $x = 0.875$ which was omitted.

Low data-transfer rates from recorder to computer as well as slow computer evaluation of the Doppler frequency resulted in a dead time of $\approx 0.1$ s between the start of digitization of a signal and the rearming of the recorder for the next Doppler burst. The maximum data rate possible was therefore $\approx 10$ Hz, with typical data rates ranging from 8 Hz in the free-stream region to less than 2 Hz in the near-wall region. The low data rates do not imply any time-averaging or low-pass filtering of the velocity signal. Rather it should be viewed as the practically instantaneous capture of a sporadic signal. Frequency and phase information *within* a phase bin (see below) are lost, but statistical moments can be reliably estimated. At such low data rates, turbulent fluctuations cannot be distinguished from high-frequency irrotational fluctuations, but in the highly turbulent shear-layer and recirculation regions of primary interest here, this should not pose a major problem.

### 2.3. *Phase definition*

Phase information was deduced from a pressure signal, taken from a tap at the centre of a cylinder sidewall. An approximately 45 cm long tube from the cylinder tap was connected to a channel tap, which, in turn, was connected to a Kistler 701A piezoelectric pressure transducer. The transducer signal was low-pass filtered at 3 Hz (cf. $f_s \approx 1.8$ Hz) in order to provide a usable phase reference, and subsequently digitized by one channel of a second 'pressure' two-channel Vuko VKS 220-16 transient recorder, with a buffer size of 8 Kbytes per channel. To perform the phase-sorting, the irregularly spaced in time, discretely sampled velocity measurement must be related in time to the quasi-continuous pressure signal. Whenever the LDV transient recorder was triggered by a Doppler burst, a pulse was outputted to the second channel of the 'pressure' transient recorder. This time-stamping related directly the instant in time when a possible velocity event occurred to the time history of the pressure signal. The components of the measurement system are schematically drawn in figure 2. When the buffers of the 'pressure' recorder were filled, the data were transferred to the computer, where the local period for each shedding cycle was determined using a peak-finding algorithm. A phase-definition based on peaks was chosen as being more immune to noise and drift as well as variations in signal amplitude, since peaks could be defined independent of any reference level. Before sorting in phase bins, the local period so determined was further checked; if the estimated period was too large ($> 2/f_s$) or too small ($< 0.5/f_s$), which might occur due to the presence of dubious peaks, velocity data within that period were discarded. Typically, less than 10% of the recorded data were rejected for this reason. The local period was then divided into 20 equal-sized intervals or phase-bins (cf. 16 phase bins were used by both Cantwell & Coles 1983 and Perry & Steiner 1987). Validated velocity measurements were then sorted according to the time at which they were acquired in relation to the phase of the pressure signal. An extract from typical synchronized velocity and pressure signal time

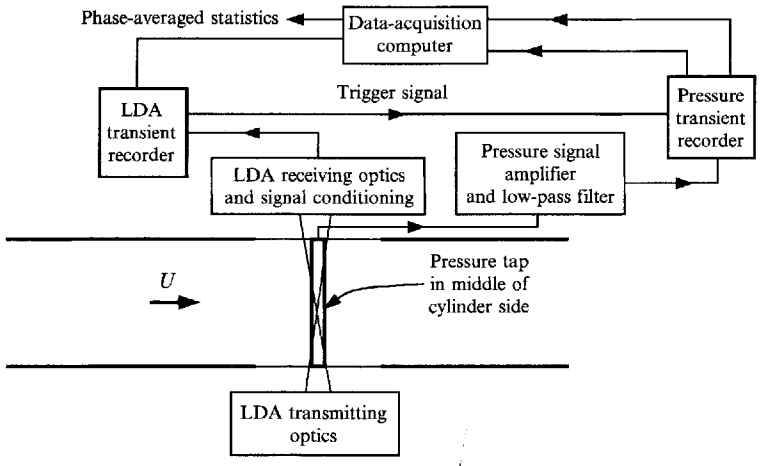


FIGURE 2. Schematic diagram of experimental set-up.

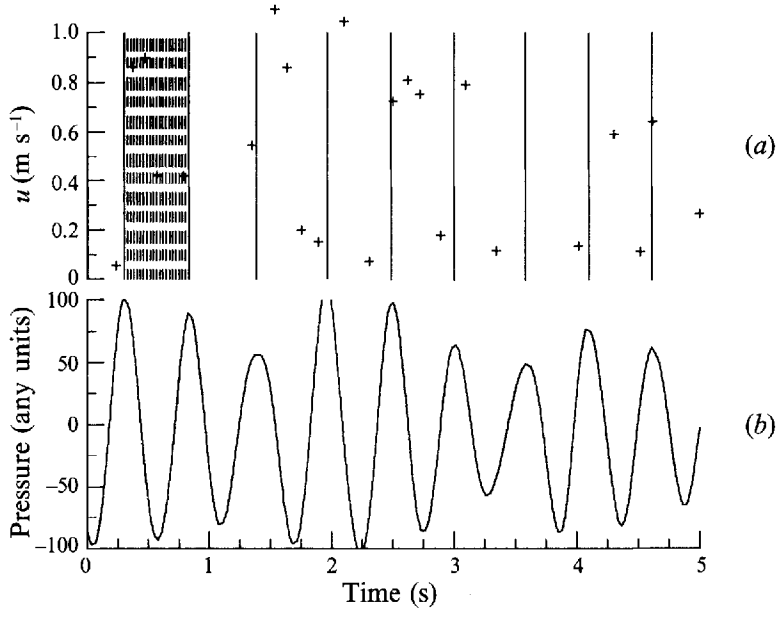


FIGURE 3. Time series of (*a*) one-component LDV realizatons, +, (average data rate ≈ 4 Hz), together with period and phase boundaries; (*b*) low-pass-filtered pressure signal (digitization rate = 400 Hz).

series is shown in figure 3, together with the defined periods and the boundaries of the phase bins.

The choice of 20 phase bins implied a bin width of ≈ 28 ms, since the average shedding period is ≈ 0.56 s. The bin width was thus significantly smaller than the dead time of the LDV velocity recorder (≈ 100 ms). Successive velocity events were therefore necessarily placed in different bins, and so conventional arithmetic averaging for each separate bin was free from LDV bias due to a possible correlation between local velocity and the number of velocity events recorded. Because the 'pressure' transient recorder acted as the synchronizing clock, a digitization rate of 400 Hz,

corresponding to a time resolution of 2.5 ms, was considered adequate. The 8-Kbyte buffer allowed a 20 s uninterrupted measuring period, which was repeated until each phase bin contained a specified number of samples. This was varied according to the expected turbulence level. In the region outside the separated shear layer where the turbulence level was relatively low, a minimum sample of 300 was specified. In and below the shear layer, a sample of 400 or 500 was required. This may be compared with 1024 samples per bin of Cantwell & Coles (1983), and the 50 samples per bin of Perry & Steiner (1987). A typical error in the $\langle u \rangle$ and $\langle u' \rangle$ of less than 0.05 is expected. Because of the large sample size desired, long measuring times were required, with a range from 30–150 minutes, or in terms of shedding cycles, 3000–16000 cycles. Since the phase reference is internal, the number of phase bins does not have any absolute significance. For convenience in the following, phase will be referred to in terms of the bin number rather than in terms of angles. For orientation purposes in considering the results, the first half-cycle (the first ten bins) corresponds approximately to an accelerating free stream, while the second half-cycle (the latter ten bins) corresponds roughly to a decelerating free stream.

## 3. Results

### 3.1. *Velocity and turbulence intensity profiles*

The deviation of phase-averaged velocity ($\langle u \rangle$) profiles for the time-averaged ($\bar{u}$) profiles is illustrated in figure 4 for two selected phases, one during an accelerating (phase 5) and one during a decelerating phase (phase 15). At the upstream section, $x = 0$, deviations are relatively small; in contrast, at the downstream section, $x = 1$, maximum-to-minimum excursions of $\langle u \rangle$ at a point may exceed 1. Deviations are largest in the shear layer, the free-stream side being relatively undisturbed, and the wall-side being inhibited by the solid boundary. A pronounced jet-like nose or bulge is formed with the maximum $\langle u \rangle$ noticeably exceeding the free-stream velocity, particularly in the region nearer to the separation point during an accelerating phase, but less so further downstream and during decelerating phase. Unlike the case of an unforced plane mixing layer, velocity gradients above the location of the velocity maximum may remain significant. The jet-like nose, also evident in the profiles of $\bar{u}$, is also observed in steady separated flows (in a normal-plate–splitter-plate flow, Ruderich & Fernholz 1986; in a bluff-plate flow, Djilali & Gartshore 1991). Gaster *et al.* (1985) also noted a very weak nose in a forced plane mixing layer. The magnitudes of the maximum $\bar{u}$ are also comparable to those in other steady separated flows.

Because the closest measuring points were typically 3 mm from the cylinder wall, the maximum negative $\langle u \rangle$ may not have been measured, particularly during an accelerating phase, when the vertical scale of the flow is very compressed. Maximum negative values of $\bar{u}$, $\approx -0.3$, are nevertheless comparable to those reported for steady bluff-plate flow (Kiya & Sasaki 1983; Djilali & Gartshore 1991). Since $\bar{u}$ at the measurement points closest to the cylinder are all clearly negative, time-averaged reattachment is unlikely to have occurred. At $(x, y) = (1, 0.075)$, a small positive $\langle u \rangle$ ($= 0.007$) was measured for a single phase (phase 5, an accelerating phase). Although this might indicate possible reattachment in the phase-averaged sense, it is likely that negative $\langle u \rangle$ closer to the cylinder occurred but was not measured. Djilali & Gartshore (1991) noted that the instantaneous reattachment point of the nominally steady bluff-plate flow is also highly mobile, and that, even in the middle of the region with the largest mean reverse flow, there was a finite probability of observing forward flow.

The corresponding profiles of $u'_0$ and $\langle u' \rangle$ are plotted in figure 5(*a*). The peak values

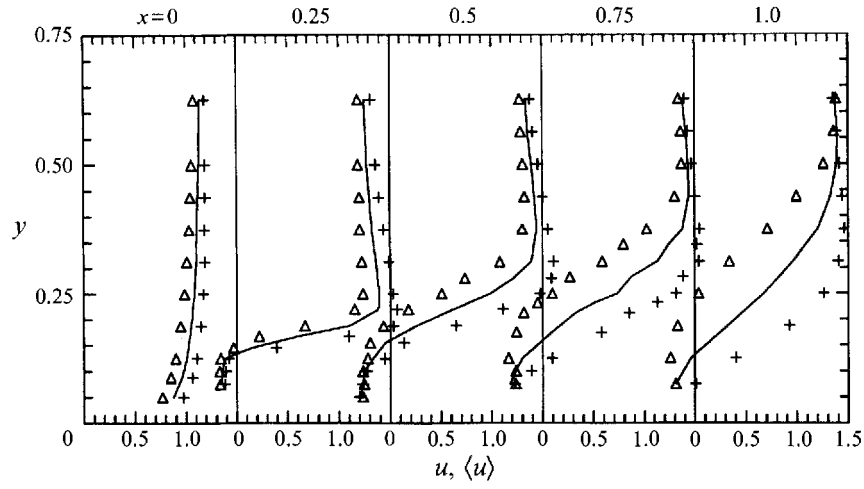


FIGURE 4. Comparison of time-averaged velocity, $\bar{u}$, profiles (solid line) with phase-averaged velocity, $\langle u \rangle$, profiles: +, phase 5; △, phase 15.

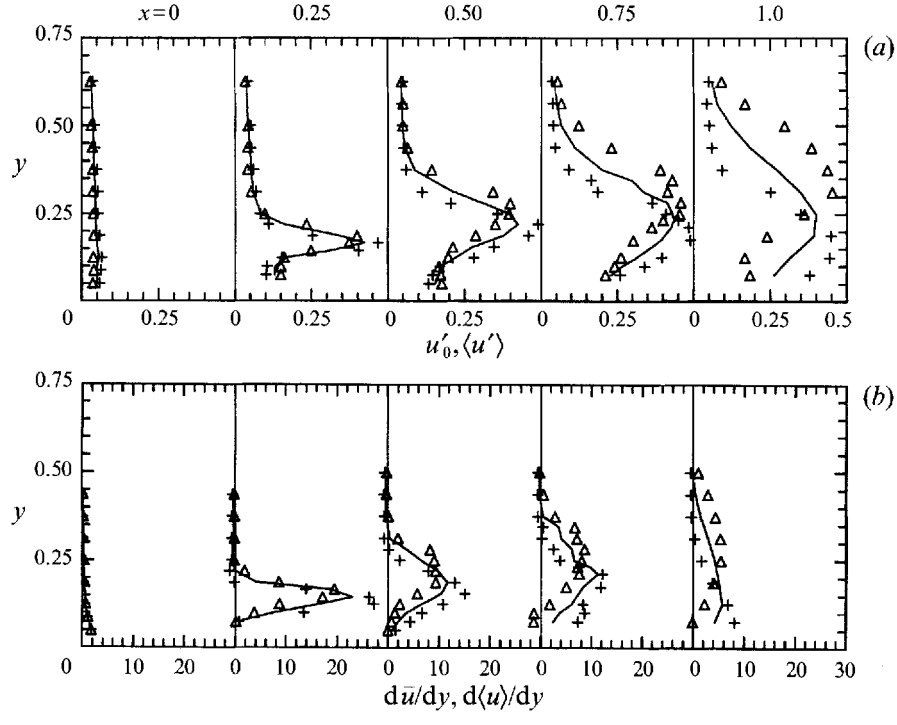


FIGURE 5. Comparison of averaged (either over all phases or over time) profiles (solid line) with phase-averaged profiles: +, phase 5; △, phase 15. (*a*) Turbulence intensity, $u'_0$, $\langle u' \rangle$; (*b*) velocity gradient, $d\bar{u}/dy$, $d\langle u \rangle/dy$.

of $u'_0$ remain approximately the same at a value, $\approx 0.4$, which is significantly higher than those of the separated bluff-plate flow ($\approx 0.3$). Maximum values of $\langle u' \rangle$ may be 10%–15% larger still than maximum values of $u'_0$, which should be considered in any comparison with the results of more simplified approaches, e.g. the spectral estimates of Fiedler & Mensing (1985), or the filtering approach of Durao *et al.* (1988). The lateral width of the $\langle u' \rangle$-profiles is correspondingly smaller than that of the $u'_0$-profiles.

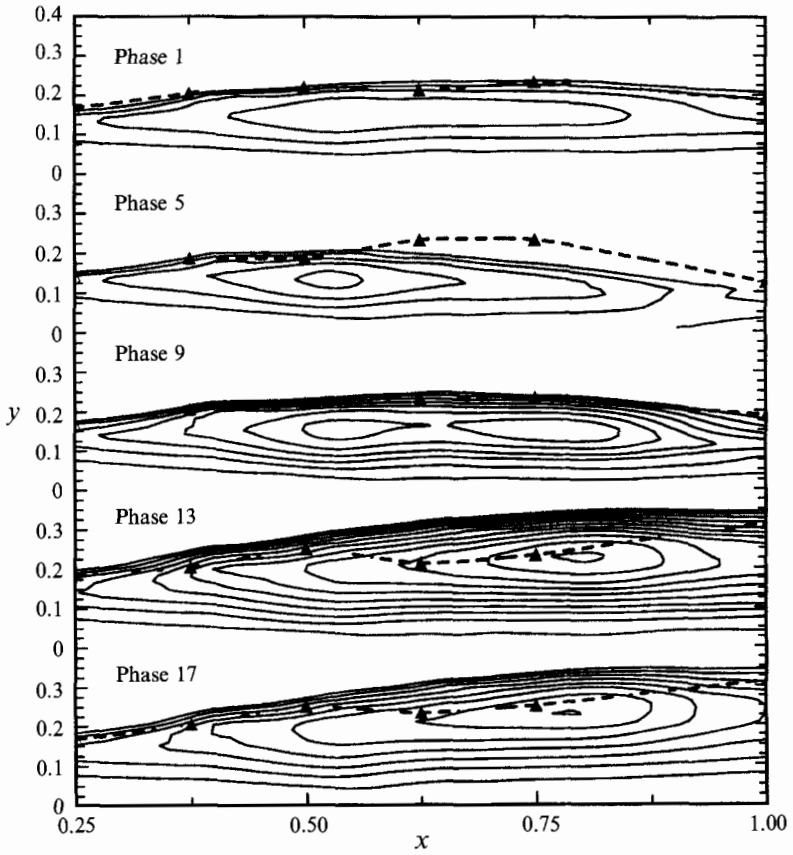


FIGURE 6. Phase-averaged streamlines of recirculating region at various phases; contours decrease from 0 in 0.006 decrements. ▲, Locations of maximum gradients of phase-averaged velocity, $(\mathrm{d}\langle u\rangle/\mathrm{d}y)_{max}$ (dashed line only a visual aid).

The vertical motion of the peak of the $\langle u'\rangle$-profiles reflects the vertical motion of the phase-averaged shear layer. This information is lost in the $u_0'$-profile, which misleadingly indicates a peak at midheight between the highest and lowest phased-averaged peaks. The gradient of $\langle u\rangle$, $\mathrm{d}\langle u\rangle/\mathrm{d}y$, is of interest since it is traditionally related to gradient transport models and may also approximate the phase-averaged vorticity in shear layers. $\mathrm{d}\langle u\rangle/\mathrm{d}y$ was estimated from measurements at three points, by interpolating a quadratic through the $\langle u\rangle$-values and assigning the gradient of the quadratic at the middle point to be the $\mathrm{d}\langle u\rangle/\mathrm{d}y$ at that point. The profiles of $\mathrm{d}\bar{u}/\mathrm{d}y$ and $\mathrm{d}\langle u\rangle/\mathrm{d}y$ (figure 5*b*) reflect the same type of vertical motion, and suggest a strong correlation between $\langle u'\rangle$ and $\mathrm{d}\langle u\rangle/\mathrm{d}y$. Peak values of both $\langle u'\rangle$ and $\mathrm{d}\langle u\rangle/\mathrm{d}y$ are larger during the acceleration than the deceleration phase, with both peaks being displaced below the peak in the average over all phases. The widths of $\langle u'\rangle$- and $\mathrm{d}\langle u\rangle/\mathrm{d}y$-profiles are also comparable.

### 3.2. *Phase-averaged streamlines and contours of* $\langle u'^2\rangle$

A picture of the phase-averaged flow field is provided by the phase-averaged streamlines (figure 6) in the body frame of reference. Streamlines are not Galilean invariant and features may depend sensitively on the reference frame used in computing the streamlines. The body frame was chosen because it corresponds to the

physical system, and a more relevant reference frame is not obvious because, as will be seen, a variety of phase velocities are observed. Streamlines were estimated by integrating a $\langle u \rangle$-profile from the cylinder sidewall, which is necessarily a streamline. For the purposes of the integration, $\langle u \rangle$ was assumed to vary linearly in the region between the wall and the closest measurement point to the wall. This introduces some error in the estimation of stream-function values, but because of the thinness of this region, the error is expected to be small away from the wall. The integration was carried out to a point where the value of the stream function vanished, which will be referred to as the separation streamline since it is the phase-averaged streamline passing through the separation point. Streamlines for $x < 0.25$ could not be estimated because of inadequate vertical resolution, and therefore are not presented. The details of the streamline plots should be interpreted cautiously since these are based on interpolation of a somewhat coarse streamwise grid.

During an accelerating phase, e.g. phase 5, the separation streamline is located close to the wall, and is directed downwards at the downstream boundary; the centre of the recirculation region is thus situated at $x \approx 0.5$. In contrast, during a decelerating phase, e.g. phase 13, the separation streamline is noticeably raised, and the centre of the recirculation region is displaced farther downstream. The volume flux passing through the downstream boundary into the recirculation region is estimated as the minimum value of the streamfunction attained in the integration of the profile at $x = 1$. This value for phase 13 was $-0.043$, which may be compared with the corresponding value for phase 1, $-0.013$. At an intermediate phase (phase 9), two eddy 'centres' are found. The term centre refers to points of zero velocity in the interior of the flow characterized by closed streamlines. In the body frame of reference they need not necessarily be associated with large-scale structures. The transition from an upstream-centred eddy to a downstream-centred eddy is completed within a relatively short interval, typically within two or three phases, and coincides approximately with the transition from an accelerating to a decelerating free-stream flow. Before and after this transition, the position of the centres is quite stable, varying little over seven or eight phases. Also shown are the cross-stream locations of the maxima in $\mathrm{d}\langle u \rangle/\mathrm{d}y$, $(\mathrm{d}\langle u \rangle/\mathrm{d}y)_{max}$, at each measurement section, which indicate roughly the location of the shear layer. During the acceleration half-cycle, these maxima coincide approximately with the separation streamline over the entire region, lying above the eddy centres. During the deceleration half-cycle, however, $(\mathrm{d}\langle u \rangle/\mathrm{d}y)_{max}$ are observed significantly below the separation streamline, quite close to the eddy centres, particularly in the downstream half of the measurement region. The association of a shear layer originating from the separation point with $(\mathrm{d}\langle u \rangle/\mathrm{d}y)_{max}$ may however be rather tenuous during decelerating phases.

The contours of the phase-averaged normal Reynolds stress, $\langle u'^2 \rangle$, are shown in figure 7. A large difference in $\langle u'^2 \rangle$ between various phases is seen, e.g. the two-fold increase between phase 1 (or phase 17) and phase 9. The largest values of $\langle u'^2 \rangle$ occur during the transition from accelerating to decelerating free stream (roughly phases 8–12), while the minimum values occur during the reverse transition (roughly phases 17–20). In nominally steady flows, contours generally exhibit an increase to a peak value, and then a subsequent decrease with downstream distance. The contours for the present flow show, however, persistent multiple local peaks. While the acceleration phases exhibit maxima in $\langle u'^2 \rangle$ in the interior of the region, in the transitional and early deceleration phases such as phases 9 and 13, the maxima occur at the downstream boundary. A close relation between $(\mathrm{d}\langle u \rangle/\mathrm{d}y)_{max}$ and $\langle u'^2 \rangle$ is seen. Even in the downstream region during the deceleration regions, when $(\mathrm{d}\langle u \rangle/\mathrm{d}y)_{max}$ lie significantly below the separation streamline, they remain rather close to the maxima in $\langle u'^2 \rangle$, e.g.

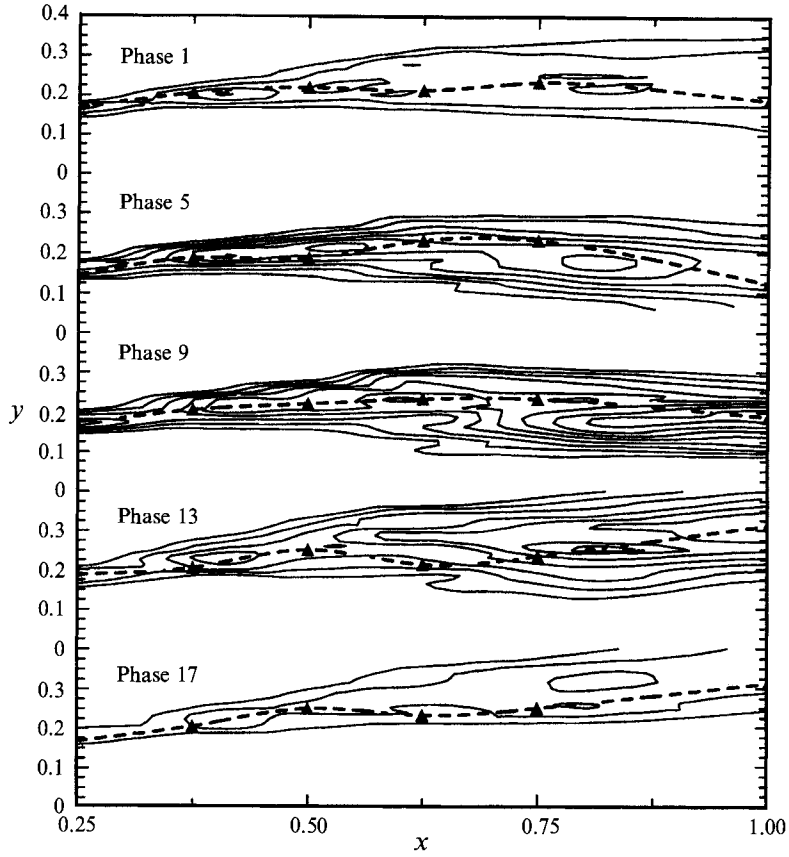


FIGURE 7. Contours of the phase-averaged normal Reynolds stress, $\langle u'^2 \rangle$, at various phases; contours increase from 0.1 in 0.03 increments. ▲, Locations of maximum gradients of phase-averaged velocity, $(\mathrm{d}\langle u \rangle/\mathrm{d}y)_{max}$ (dashed line only a visual aid).

in phase 13. Compared to the phase-averaged streamlines (figure 6), contours of high $\langle u'^2 \rangle$ are distributed about the line of $(\mathrm{d}\langle u \rangle/\mathrm{d}y)_{max}$. During the acceleration phases, the maxima in $\langle u'^2 \rangle$ are not related to the location of eddy centres. This is, however, less clear in the downstream half of the flow region during deceleration phases, where eddy centres are associated with relatively large, if not maximal, values of $\langle u'^2 \rangle$. Large values of $\langle u'^2 \rangle$ do not necessarily imply large values of Reynolds shear stresses as is found, for example, in the phase-averaged near-wake flow; two-component measurements outside the measurement region do however indicate that large values of Reynolds shear stresses are observed in the shear-layer region.

### 3.3. *Phase variations*

In the following, the centre of the time-averaged shear-layer, $y_{sh}$, is defined as the point at which $\mathrm{d}\bar{u}/\mathrm{d}y$ attains a maximum. The edges of the mean-shear-layer are defined as the points above and below $y_{sh}$ at which $|\mathrm{d}\bar{u}/\mathrm{d}y| \leqslant 2$. Because the former point is approximately the same as the point of maximum $\bar{u}$, it is denoted as $y_{max}$, while the latter point is denoted $y_{min}$, since it occurs near the minimum $\bar{u}$. Unlike the unforced mixing layer, where $y_{max}$ also approximately marks the free stream, in the present case where a pronounced jet-like bulge is observed in the velocity profile, $y_{max}$ should be distinguished from the approach to the free stream, $y_{fs}$, which is taken where $u'_0$ reaches

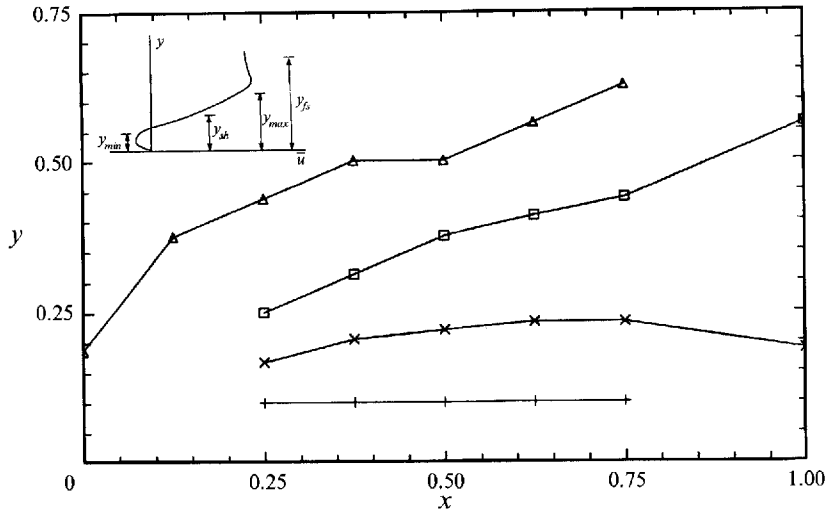


FIGURE 8. Loci of various 'characteristic' locations, based on time-averaged quantities: △, $y_{fs}$; □, $y_{max}$; ×, $y_{sh}$; +, $y_{min}$ (solid lines only a visual aid).

a value of 0.05 (cf. a free-stream turbulence level $\approx 0.02$). These characteristic locations, a loci of which are shown in figure 8, are found to be useful in discussing the phase and amplitude characteristics of the flapping shear layer, even though they are based on time-averaged quantities.

The variation of $\tilde{u}$, $\widetilde{u'}$, and $\widetilde{(\mathrm{d}u/\mathrm{d}y)}$, with phase at $x = 0.25$ is shown in figure 9. To emphasize phase rather than amplitude variations, each variable has been normalized by half of the difference between the maximum and minimum value attained. The variation in $\tilde{u}$ is quite smooth everywhere except possibly at the points closest to the cylinder, which indicates that the sample size for phase averaging was sufficient to obtain stable averages for $\tilde{u}$. The phase variation in $\widetilde{u'}$ is more erratic. At some points this is due to the small amplitudes, e.g. at $y = 0.5 \approx y_{fs}$ amplitudes are typically 1%–2% of $\bar{u}$, which is at the uncertainty limits of the measurements. At other points, larger scatter is associated with a transition in behaviour, e.g. at $y = 0.25 \approx y_{max}$ a change in phase behaviour of $\widetilde{u'}$ and $\widetilde{(\mathrm{d}u/\mathrm{d}y)}$ is observed, and is accompanied by erratic behaviour of $\widetilde{u'}$ and $\widetilde{(\mathrm{d}u/\mathrm{d}y)}$.

In the neighbourhood of $y = 0.5 \approx y_{fs}$, the phase variation of both $\tilde{u}$ and $\widetilde{u'}$ exhibits essentially the first harmonic, and both vary in phase with each other. A similar phase relationship between $\tilde{u}$ and $\widetilde{u'}$ is found outside the unsteady attached boundary layer (Cousteix & Houdeville 1988). In contrast, $\widetilde{(\mathrm{d}u/\mathrm{d}y)}$ is directly out of phase with $\widetilde{u'}$. As the shear layer is approached from above, i.e. near $y = 0.25 \approx y_{max}$, a transition is observed in the variation of $\widetilde{u'}$; higher harmonics become important, and its phase diverges from that of $\tilde{u}$. The phase difference between $\widetilde{(\mathrm{d}u/\mathrm{d}y)}$ and $\widetilde{u'}$ narrows, however. The transition is completed by $y = 0.188$, where $\widetilde{u'}$ again assumes a smoother form, and varies in phase with $\widetilde{(\mathrm{d}u/\mathrm{d}y)}$. At the next lower measurement point, $y = 0.168 \approx y_{sh}$, a sharp change in the phase of $\widetilde{u'}$ occurs, while the phase of $\tilde{u}$ has changed little. The sharp change in phase of $\widetilde{u'}$ is however accompanied by a similar change in phase of $\widetilde{(\mathrm{d}u/\mathrm{d}y)}$ such that the two remain in phase. All remain in phase until closer to the cylinder wall, when, at $y = 0.1 \approx y_{min}$, $\langle u' \rangle$ goes again out of phase with both $\tilde{u}$ and $\widetilde{(\mathrm{d}u/\mathrm{d}y)}$, both of which remain approximately in phase.

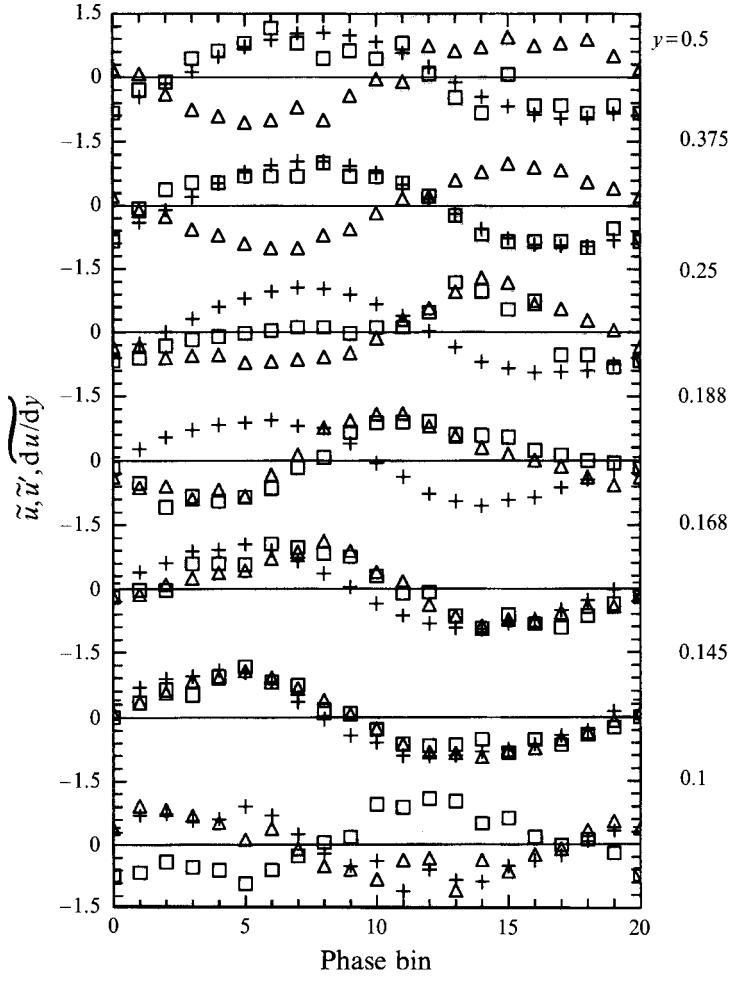


FIGURE 9. Comparison of variation with phase at different vertical positions for $x = 0.25$ of +, $\tilde{u}$; □, $\tilde{u}'$; △, $(\overline{du/dy})$.

### 3.4. *Amplitude profiles*

The amplitude and phase of the first-harmonic component may be used to characterize the major features of periodic signals. Although figure 9 indiates that higher-order harmonics are not everywhere negligible, their estimation involves greater uncertainty, and their implications are less clear, so the following discussion is restricted to first harmonics. The first-harmonic amplitude and phase are denoted by a subscript 1; for example, for $\tilde{u}$,

$$\tilde{u} \approx u_1 \cos(2\pi f_s t - \alpha_1), \tag{2}$$

where $u_1$ and $\alpha_1$ are the amplitude and phase of the first harmonic and $f_s$ is the vortex shedding frequency. The $u_1$-profile has a single maximum occurring close to $y_{sh}$, and flattens out rather abruptly above $y_{max}$ (figure 10). The maximum value and particularly the width (roughly, $2(y_{max} - y_{sh})$) grow with downstream distance. In contrast, the $u_1'$-profiles exhibit a bimodal distribution, which becomes evident as early as $x = 0.375$. The maximal amplitudes, as well as the distance between local maxima, grow with $x$. The maximum in $u_1$, i.e. where the gradient of $u_1$ vanishes, coincides with

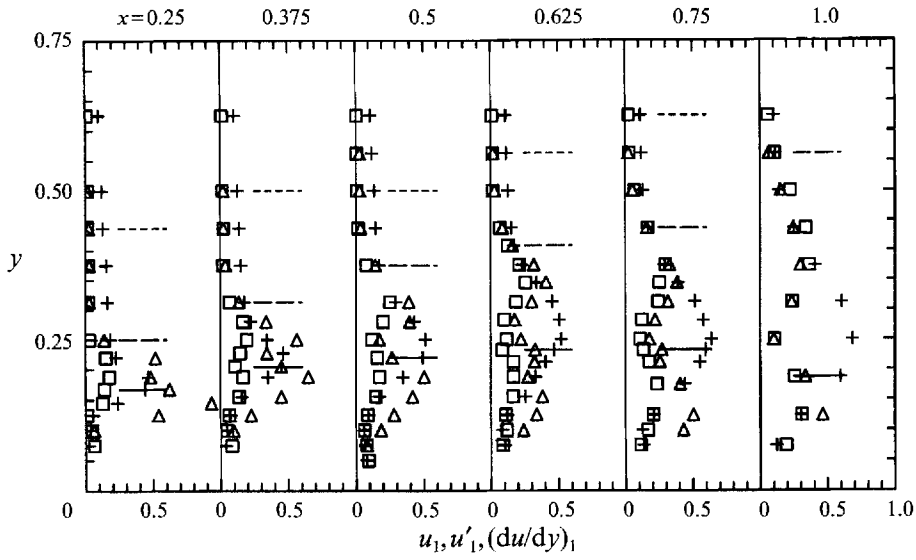


FIGURE 10. Amplitude (first harmonic) profiles: +, $u_1$; □, $2\times u_1'$; △, $0.1\times(\mathrm{d}u/\mathrm{d}y)_1$; ——, $y=y_{sh}$; – – –, $y=y_{max}$; ·····, $y=y_{fs}$.

the local minimum in $u_1'$. Further, local maxima in $u_1'$ are situated where the magnitude of the gradients of the $u_1$ are largest. Peaks and valleys of $(\mathrm{d}u/\mathrm{d}y)_1$ and $u_1'$ also coincide.

At a fixed vertical location near $y_{sh}$, vertical movements of the unsteady shear layer result in large oscillations in $\langle u\rangle$, and hence large $u_1$, because of large velocity gradients. The width of the $u_1$-profile indicates the range of the oscillation; downstream growth of the width reflects the growth in the range of the flapping motion, which in turn also influences the maximum amplitude, since the larger the range, the greater the difference in velocities expected at a fixed point. Because the unsteady shear layer spends most of the time in the neighbourhood of $y_{sh}$, $u_0'$ is high; the amplitude about $u_0'$ at $y_{sh}$ will however be relatively small. Maximum values of $u_1'$ are expected, rather, at points which are immersed, during one part of the cycle, in the free stream (or in the low-shear region closer to the wall) and hence experience low $\langle u'\rangle$, and, during another part of the cycle, in the shear layer, and hence experience high $\langle u'\rangle$. These points will be found flanking, but not at, $y_{sh}$. This would also be consistent with the coincidence of maxima of $\langle u'\rangle$- and $\mathrm{d}\langle u\rangle/\mathrm{d}y$-profiles, since the shear layer is identified with both large $\langle u'\rangle$ and large $\mathrm{d}\langle u\rangle/\mathrm{d}y$.

### 3.5. *Phase-angle profiles*

The profiles of the phase angles for $\tilde{u}$, $\widetilde{u'}$, and $\widetilde{(\mathrm{d}u/\mathrm{d}y)}$, denoted as $\alpha_1$, $\beta_1$, and $\gamma_1$ respectively (where appropriate, $2\pi$ has been added or subtracted), are shown in figure 11. At the leading edge (not shown), $\alpha_1$ and $\beta_1$ coincide and are essentially independent of distance from the cylinder. This remains the case up to $x=0.375$ for the region above $y_{max}$. A layered vertical structure is observed by $x=0.25$ for $\alpha_1$, with $y_{max}$ associated with the beginning of the transition layer, and $y_{sh}$ in the centre of the transition layer. By $x=0.5$, a three-layer structure becomes evident, where $\alpha_1$ remains approximately constant within each layer, and changes rapidly between layers. While $y_{max}$ continues to mark an upper transition, $y_{sh}$ is found roughly at the centre of an intermediate layer rather than a transition layer, and a lower transition is observed near $y_{min}$. The central layer grows in width with downstream distance at about the

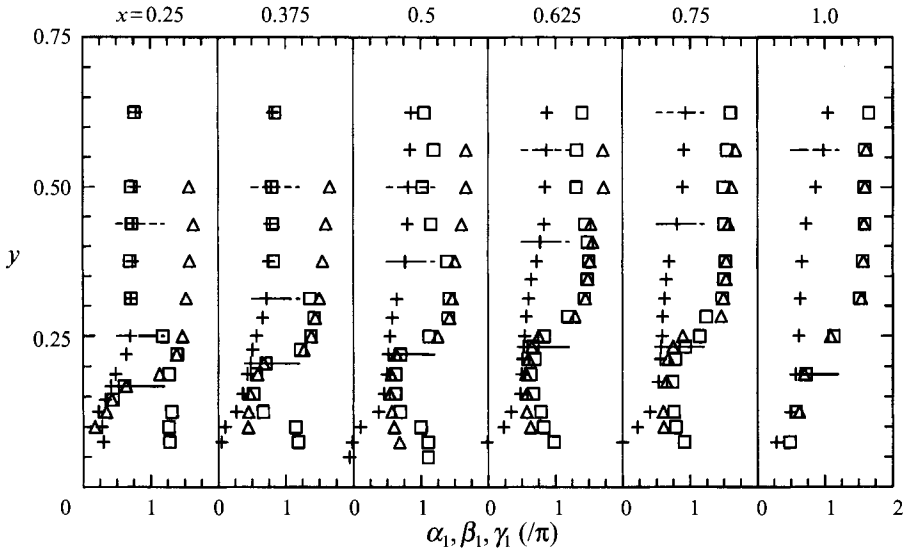


FIGURE 11. Phase (first harmonic) profiles: +, $\alpha_1(\langle u\rangle)$; □, $\beta_1(\langle u'\rangle)$; △, $\gamma_1(\mathrm{d}\langle u\rangle/\mathrm{d}y)_1$; ——, $y = y_{sh}$; – – –, $y = y_{max}$; · · · · · · · · ·, $y = y_{fs}$.

same rate as the mean shear layer such that, by $x = 1$, it has almost completely displaced the upper and lower layers.

The characteristic locations, $y_{max}$, $y_{sh}$, and $y_{min}$, retain their significance in the structure of the $\beta_1$-profile. Up to $x = 0.375$, $\beta_1$ is relatively constant for $y > y_{max}$ and for $y_{max} > y > y_{ah}$, but varies rapidly in the vicinity of both $y_{max}$ and $y_{sh}$ and also near $y_{min}$. By $x = 1$, however, these features have been smeared out, with $\beta_1$ remaining almost constant from the middle of shear-layer region upwards. Unlike $\alpha_1$ and $\beta_1$, $\gamma_1$ varies little with distance downstream in the free-stream region. It is initially directly out of phase with $\beta_1$ (and hence with $\alpha_1$). At $x = 0.25$, a large gradient in $\gamma_1$ appears at $y_{sh}$, which is not significantly reduced downstream until $x = 1$. In quite substantial regions of the flow, the difference between $\beta_1$ and $\gamma_1$ is practically zero. At $x = 0.25$, this region of practically zero phase difference is limited to $0.1 < y < 0.2$, but by $x = 1$ it has grown to encompass the entire region where estimates of $(\mathrm{d}u/\mathrm{d}y)$ were made.

Phase is determined in large part by the points in time when the cyclic maximum and minimum occur. If, in any region with significant velocity gradients, the sign of the profile gradient does not change during the cycle, then, with a vertically oscillating shear layer, large rapid changes in phase are unlikely to be found because cyclic maxima and minima tend to occur at approximately the same time. Thus, in the shear layer or in the free-stream region, $\alpha_1$ varies very little vertically. In regions where profile extrema occur, the sign of the gradient may change during a cycle due to vertical movement of the profile extrema. The point in time at which a cyclic maximum occurs may therefore vary substantially. Thus, the major transitions in $\alpha_1$ tend to occur in the neighbourhood of $y_{max}$ and $y_{min}$. Similarly, because the $\langle u'\rangle$-profile is very peaked, vertical movement of the profile maximum of $\langle u'\rangle$ results in vertical variations in $\beta_1$. Since these peaks occur in the shear-layer region, the region of large rapid variation in $\beta_1$ near $y_{sh}$ can be so explained. The transitions of $\beta_1$ near $y_{max}$ and $y_{min}$ do not fit this picture. These are attributed rather to phase relationships between local turbulence conditions not directly determined by the effect of vertical shear-layer movement on $\langle u'\rangle$, possibly due to detailed flow features such as the jet-like bulge, or to turbulence convected from the wake region.

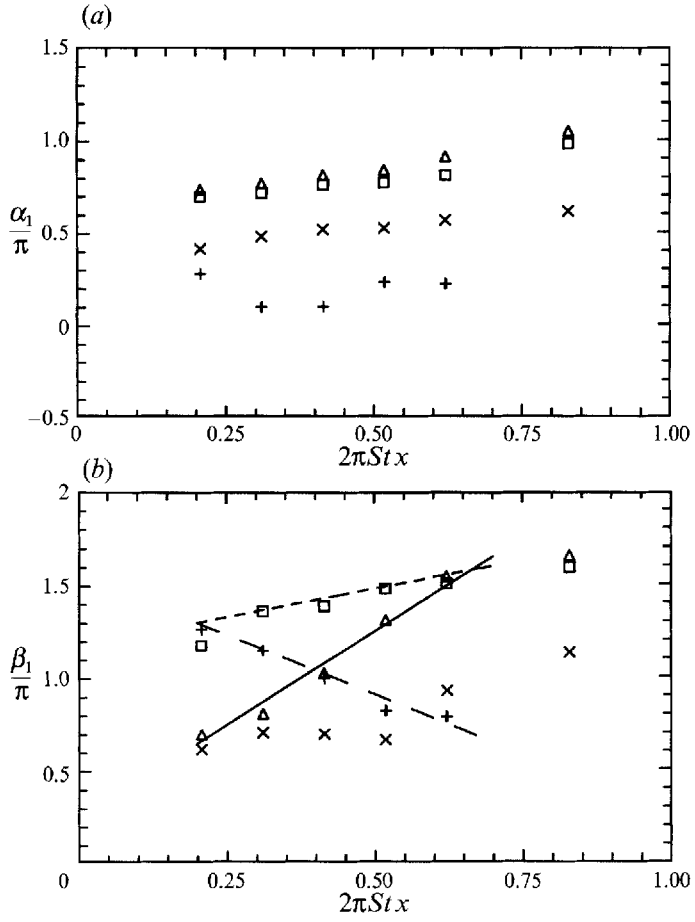


FIGURE 12. Streamwise variation of (first harmonic) phase angles of (*a*) $\langle u \rangle$ and (*b*) $\langle u' \rangle$ at the different characteristic locations: △, $y = y_{fs}$; □, $y = y_{max}$; ×, $y = y_{sh}$; +, $y = y_{min}$; – – – –, phase velocity $\approx -0.5$; ——, phase velocity $\approx 1$; ·····, phase velocity $\approx 0.35$.

### 3.6. *Streamwise variation of phase angles*

An estimate of phase (convection) velocities can be made from the streamwise variation of phase angles at characteristic locations if they vary linearly. For the unsteady boundary layer, Cousteix & Houdeville (1988) considered points where $y/\bar{\delta} =$ constant, where $\bar{\delta}$ is the time-averaged boundary-layer thickness. Similarly, Gaster *et al.* (1985) chose points defined in terms of the time-averaged velocity profiles. In the preceding discussion, locations such as $y_{max}$ and $y_{sh}$ were useful in marking transitions, and are therefore used in examining the streamwise variation of phase angles. The variation of $\alpha_1$ with the dimensionless streamwise distance, $2\pi Stx$, is plotted in figure 12(*a*). Although the variation along all points except $y_{min}$ is roughly linear over the limited measurement region, the phase velocities (estimated from the reciprocal of the slopes) are much larger ($\approx$ 2–2.5) than physical velocities. While $\alpha_1$ along $y_{fs}$ grows slowly, $\alpha_1$ along $y_{min}$ decreases more rapidly at first, but then becomes constant or only very slow varying. The streamwise variation of $\beta_1$ depends sensitively on vertical location (figure 12*b*). Along $y_{sh}$ it is negligible, but along other characteristic points, $\beta_1$ varies approximately linearly within $0.25 \leqslant x \leqslant 0.75$ associated, however, with disparate phase velocities. The associated phase velocity along $y_{min}$ is negative, as

would be appropriate for a reverse-flow region, with a value of $\approx -0.4$ to $-0.5$ (cf. a typical peak $u_0$, which ranged from $-0.2$ to $-0.3$, and the maximum negative $\langle u \rangle$ measured, $-0.52$). These values give some support to the importance of convective processes in determining phase relationships of $\beta_1$. Along $y_{max}$, the phase velocity is positive, with a magnitude of $\approx 1$, which is 70% of $u_0 \approx 1.4$ and 60% of the maximum $\langle u \rangle \approx 1.65$. Finally, along $y_{fs}$, phase velocities are reduced even further, with values, $\approx 0.3$, indicative perhaps of even larger structures.

### 3.7. *Comparison with previous flow studies*

In phase-averaged velocity measurements of a forced turbulent plane mixing layer, Gaster *et al.* (1985) observed and predicted theoretically from linear stability analysis a dominant central peak in the disturbance amplitude in the near field. A three-layer structure in the phase-angle profiles was also predicted and observed with transitions occurring in the vicinity of the edges of the shear layer. Unlike the present results, however, strong sidelobes in the amplitude profile developed farther downstream, and phase velocities varied only slightly across the layer, with magnitudes similar to that of the unforced case. In spite of some similarities between the present case and the forced mixing layer, a direct analogy as far as the detailed mechanism of flow development is concerned remains rather tenuous. For a nominally steady bluff-plate flow in the reattachment region, Kiya & Sasaki (1983) reported phase velocities of $\approx 0.7$ in the neighbourhood of the reattachment region, but again only weakly varying with distance from the plate. Such flow regions are dominated by a single type of large structure, moving within a narrow range of velocities. In unsteady attached boundary layers, phase velocities in the outer flow have been estimated to be $\approx 70\%$–$80\%$ of the time-averaged free-stream velocity (Cousteix & Houdeville 1988), comparable to the present case. In the log layer, however, not only is the phase angle constant but phase velocities are very large. This behaviour, which reflects the multiple scales of the wall-bounded flows, seems more akin to that found in the present study. In forced boundary layers after separation (Simpson *et al.* 1983), $\alpha_1$ in the free stream and $\alpha_1$ nearer the wall diverge with downstream distance, attaining an $\approx \frac{3}{4}\pi$ phase difference between free-stream and backflow regions downstream of separation, similar to the behaviour shown in figure 12(*a*). In this respect, therefore the phase variations in the present flow behave more like the wall-bounded boundary-layer flow than a free flow.

## 4. The shear-layer region

### 4.1. *Similarity in the shear-layer region*

Figure 13(*a*) shows $\langle u \rangle$-profiles at various phases in the shear-layer region plotted in standard 'similarity' coordinates, based on fitting the profiles according to

$$\frac{\langle u \rangle - \langle u \rangle_{min}}{\langle \Delta u \rangle} = \frac{1 + \operatorname{erf} \xi}{2}, \tag{3}$$

where $\langle \Delta u \rangle \equiv \langle u \rangle_{max} - \langle u \rangle_{min}$ and $\xi = (y - \langle y_c \rangle)/\langle \delta_\xi \rangle$, the 'centre', $\langle y_c \rangle$, and the thickness, $\langle \delta_\xi \rangle$, of the shear layer, being determined by a least-squares fit. Only measurement points in the region, $|\xi| \leqslant 2$, were included in the fit, but this typically included the entire region between the maximum and minimum measured $\langle u \rangle$. The collapse is surprisingly good, with no noticeably consistent departue (2% r.m.s. error is generally achieved in the fitting) with phase or with station. This might have been expected from the constant phase angle, $\alpha_1$, in almost all of this region (figure 11).

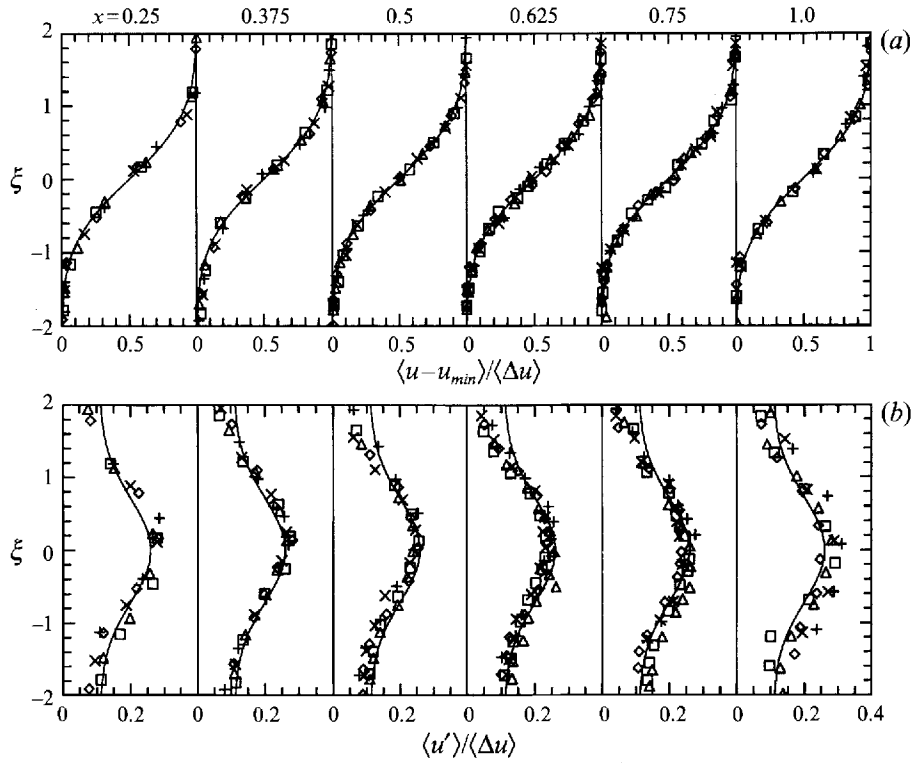


FIGURE 13. Profiles in similarity coordinates of (*a*) velocity (solid line – error function, equation (3)), and (*b*) turbulence intensity (solid line – Gaussian curve plus a constant), averaged at constant phases (every fourth plotted, each with different symbol) in the central shear-layer region.

Although some scatter in $\langle u' \rangle$ plotted in similarity coordinates (figure 13*b*) is evident, the collapse of the different phases at a specific $x$-station is, with the exception of the last section, still reasonable. An asymmetry about $\xi = 0$ is noticeable, thus differing from the steady or even forced mixing layer. For points $\xi \to 2$, $\langle u' \rangle / \langle \Delta u \rangle$ tends to be smaller than at points, $\xi \to -2$. Peaks, or regions of large $\langle u' \rangle / \langle \Delta u \rangle$, tend to be flatter and to extend above $\xi = 0$, with $\langle u' \rangle / \langle \Delta u \rangle$ thereafter decreasing more rapidly. The asymmetry is attributed to the different boundary conditions, since for $\xi \to +\infty$ the flow is the low-turbulence free stream, while for $\xi \to -\infty$ the flow is the high-turbulence recirculating flow. The collapse at different $x$-stations is less consistent. Values of $\langle u' \rangle / \langle \Delta u \rangle$ are generally larger at $x = 0.25$, decrease at first until $x \approx 0.5$, and then begin to increase thereafter. This was already seen in the contours of $\langle u' \rangle$ (figure 7), where however the normalization was different. Asymmetries also tend to be accentuated, with broad peaks being found sometimes in the upper half of the shear layer and sometimes in the lower half.

In studies of the forced mixing layer, the time-averaged velocity profile has been found to be fitted by the error function (Oster & Wygnanski 1982), but deviations (from a tanh-profile) have also been reported in regions of large-scale vortex merging (Ho & Huang 1982). A referee has pointed out that, with the present phase resolution, the $\langle u \rangle$-profiles represent an average over several cycles of the fundamental instability period. This may not necessarily imply the observations, but it points to possibilities other than an analogy between the forced mixing layer and the present flow. It is also noted that where log–law similarity prevails in forced attached boundary layers, the phase angle is also found to be constant, as in the present case (figure 11). The

asymmetry seen in the $\langle u' \rangle$-profile is also found in the steady separated shear layer with recirculation (Castro & Haque 1987). The streamwise variation in the peak values of $\langle u' \rangle / \langle \Delta u \rangle$ contrasts with the behaviour of the steady mixing layer developing towards self-preservation, which exhibits a monotonic approach to the equilibrium peak value (Mehta & Westphal 1986). Peak values of $\langle u' \rangle / \langle \Delta u \rangle$, $\approx 0.25$, are however 50% larger than those observed in steady plane mixing layers, usually $\approx 0.17$. In a forced mixing layer, Oster & Wygnanski (1982) reported peak values of $\overline{u'}/\Delta u$ of $\approx 0.2$, but this may have included a contribution due to the periodic component. They also reported double peaks in $\overline{u'}/\Delta u$ in regions of inhibited shear-layer growth. In isolated phases at $x = 0.625$, some slight evidence of double peaks in $\langle u' \rangle / \langle \Delta u \rangle$ could be found, but this was within the experimental uncertainty. Steady separated shear layers do exhibit peak values of $\overline{u'}/\Delta u$ of magnitude comparable to those measured in the present case. These are found, however, at downstream locations beyond the middle of the recirculation region (Castro & Haque 1987; Ruderich & Fernholz 1986), and not as close to the separation point as in the present case.

### 4.2. *Streamwise growth of the shear layer*

The self-similar steady plane mixing layer is characterized by a linear growth of a lateral lengthscale, which may be defined either in terms of a profile fit, $\langle \delta_\xi \rangle$, as above, or in terms of a local parameter, e.g. the vorticity thickness, $\langle \delta_\omega \rangle \equiv \Delta u_{max} / (\mathrm{d}\langle u \rangle / \mathrm{d}y)_{max}$. For steady separated shear layers with recirculation, a linear growth of $\delta_\omega$ has been observed for bluff-plate flow (Kiya & Sasaki 1983; Cherry *et al.* 1984) and normal-plate–splitter-plate flow (Ruderich & Fernholz 1986) in a region extending at least to the midpoint of the recirculation region. This has been disputed by Castro & Haque (1987), who argued that the effects of recirculation on the shear layer could not be neglected. Mixing-layer growth also varies with the velocity ratio parameter, $R \equiv (u_{max} - u_{min})/(u_{max} + u_{min})$. In the present flow, $\langle R \rangle$ ranges from 1 to 2, depending on phase and location. The streamwise development of $\langle \delta_\omega \rangle$ for various phases is compared in figure 14 to the growth of $(\delta_\omega)_0$, the average over all phases of $\langle \delta_\omega \rangle$. Even $(\delta_\omega)_0$ does not show any extensive linear growth region. After a slow-to-normal (compared to a steady separated shear layer) growth region beginning at $x = 0.25$, a rapid growth region is consistently found in $0.375 < x < 0.5$. In contrast, the region, $0.5 < x < 0.75$, may, depending on phase, exhibit growth rates that are partly slower or even negative, or partly higher than normal. Beyond $x = 0.75$, the growth rate is generally lower (greater) than normal during acceleration (deceleration). Some of this growth behaviour was reflected in the streamwise variation of $\langle u' \rangle / \langle \Delta u \rangle$ (figure 13). The noticeable decrease in values of $\langle u' \rangle / \langle \Delta u \rangle$ seen between $x = 0.75$ and $x = 1$ corresponds to the marked increase in $\langle \delta_\omega \rangle$ within the same region. Both $\langle u' \rangle$ and $\langle \delta_\omega \rangle$ are affected by $\mathrm{d}\langle u \rangle / \mathrm{d}y$, such that some relation between the two behaviours is to be expected.

Larger $\langle \delta_\omega \rangle$ values are favoured during the decelerating rather than during the accelerating phases. Accelerated flows are associated with increased flow stability since mean kinetic energy is increased at the expense of turbulent kinetic energy. The growth of the turbulent shear layer may therefore be expected to be relatively inhibited during the accelerating phase and relatively enhanced during the decelerating phase. This does not explain the observations between $x = 0.625$ and $x = 0.75$, where during an accelerating phase (phase 5) a slight increase in $\langle \delta_\omega \rangle$ occurs, but during a decelerating phase (phase 13) a slight *decrease* occurs. Such a decrease in $\langle \delta_\omega \rangle$ would require a sharpening of gradients. In a developing mixing layer before the linear regime is attained, the growth rate is typically only larger than linear, and not alternating from

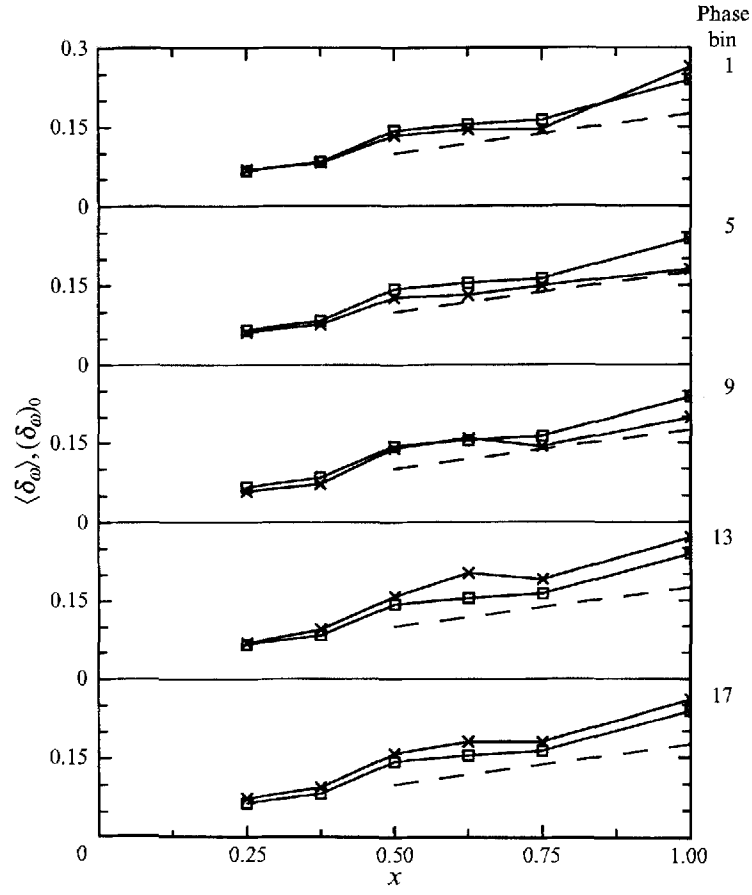


FIGURE 14. Growth of vorticity thickness: ×, phase-averaged; □, averaged over all phases (solid lines only a visual aid); ------, linear growth law for bluff-plate flow according to Djilali & Gartshore (1991).

smaller to larger to smaller (Mehta & Westphal 1986). It is reminiscent of the rather step-like growth observed in forced mixing layers (Oster & Wygnanski 1982; Ho & Huang 1982), where fast or slow growth apparently results from either enhanced or inhibited vortex merging. If the vortex shedding frequency is regarded as the 'forcing' frequency, it is much smaller than the estimated most-amplified frequency ($O(10^2)$ Hz, based on an estimated initial momentum thickness and the approach velocity). A subharmonic instability (Ho & Huang 1982) resulting from a flow for which the most amplified instability frequency is a (usually small) integral multiple of the forcing frequency is therefore an unlikely explanation. An alternative mechanism for the case of large-amplitude forcing at frequencies much lower than the most-amplified frequency has been suggested (Ho & Huang 1982), based on 'collective interaction', whereby many small vortices merge at the same time. No strong evidence of such a mechanism was found in the flow visualizations, which were however of relatively poor quality at the high Reynolds number studied, and so were not conclusive.

In steady separated shear-layer flows, the growth in shear-layer thickness tends to flatten out in the vicinity of the centre of the recirculation region (Ruderich & Fernholz 1986; Castro & Haque 1987). The streamwise location of the centre of the recirculation eddy in the present case oscillates in the streamwise direction (figure 6). In the middle

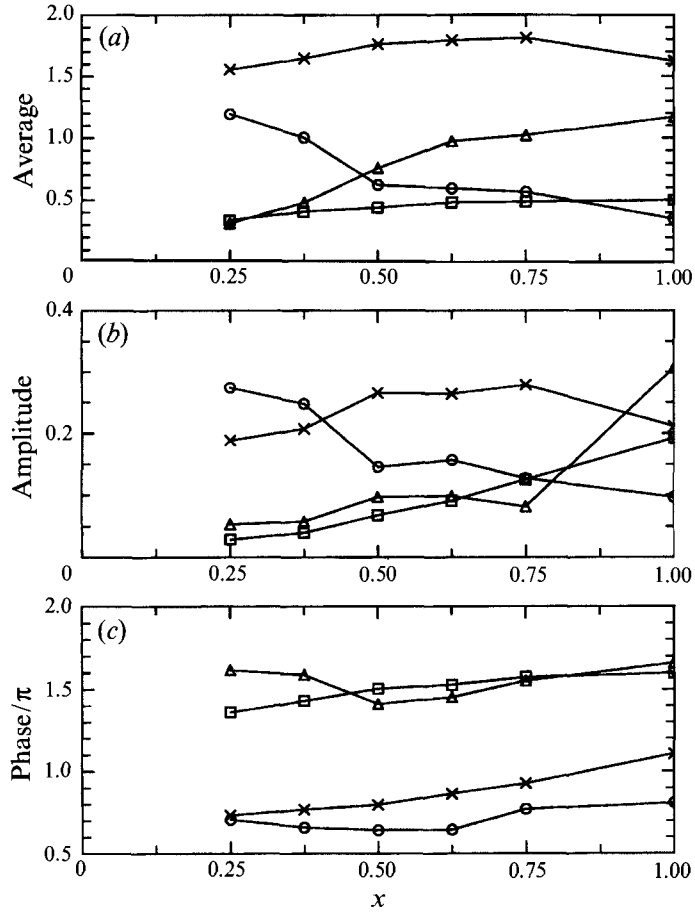


FIGURE 15. Variation of (*a*) average over all phases, (*b*) first-harmonic amplitude, and (*c*) first-harmonic phase, of the profile parameters: △, $10\times\langle\delta_\xi\rangle$; □, $2\times\langle y_c\rangle$; ×, $\langle\Delta u\rangle$; ○, $0.05\times(\mathrm{d}\langle u\rangle/\mathrm{d}y)_{max}$ (solid lines only a visual aid).

of the accelerating half-cycle (phase 5), when the eddy centre is located just beyond $x = 0.5$, the growth in $\langle\delta_\omega\rangle$ flattens out in the same region. On the other hand, in the middle of the decelerating half-cycle (phase 13), when the eddy centre has moved downstream just beyond $x = 0.75$, the slow- (or negative)-growth region is found further downstream. The free stream, which tends to depress the separation streamline, is opposed by the recirculation eddy, resulting in a funnelling effect that maintains or even sharpens velocity gradients, particularly in the region above the centre of the recirculation eddy. Consequently, the growth of the shear-layer thickness is reduced, possibly even becoming negative, in these regions.

### 4.3. *Phase variation of profile parameters*

The profile parameters, $\langle y_c\rangle$, $\langle\delta_\xi\rangle$, $(\mathrm{d}\langle u\rangle/\mathrm{d}y)_{max}$, and $\langle\Delta u\rangle$ are not similarity scales, but they provide some quantitative characterization of the phase-averaged flow field. The results of a harmonic analysis of their variation with phase (only first harmonics are considered) are summarized in figure 15. The average and the oscillation amplitude of $\langle\Delta u\rangle$ develop gradually compared to those of $(\mathrm{d}\langle u\rangle/\mathrm{d}y)_{max}$, which decrease fairly sharply for $x \leqslant 0.5$ but then level off abruptly. The development of both the average and the amplitude of $\langle\delta_\xi\rangle$, qualitatively similar to that already seen in $\langle\delta_\omega\rangle$, essentially

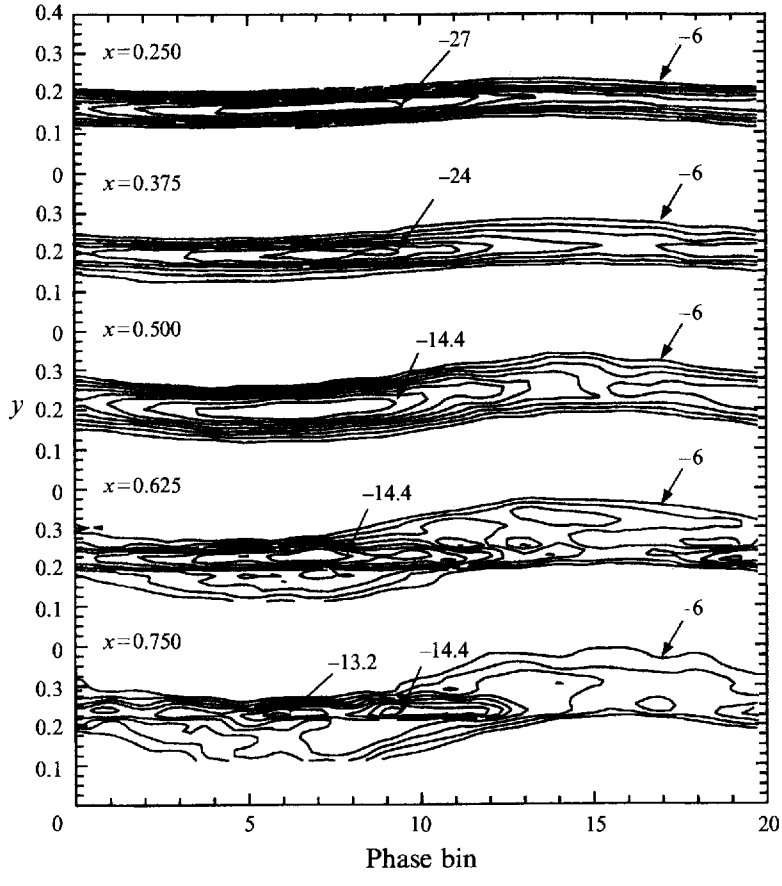


FIGURE 16. Vorticity ($= -\mathrm{d}\langle u\rangle/\mathrm{d}y$) contours at various $x$-stations as a function of phase bins; contour interval is 3 for $x \leqslant 0.375$, and 1.2 for $x > 0.375$.

reflects the influence of $(\mathrm{d}\langle u\rangle/\mathrm{d}y)_{max}$. Although $\langle y_c\rangle$ may initially lead $\langle \delta_\xi\rangle$ by as much as $\frac{1}{4}\pi$, it lags $\langle \delta_\xi\rangle$ further downstream. Phase differences are however generally slight beyond $x = 0.375$, again pointing to larger $\langle \delta_\xi\rangle$ during deceleration rather than acceleration phases. The phase relation between $\langle \Delta u\rangle$ and $(\mathrm{d}\langle u\rangle/\mathrm{d}y)_{max}$ is important in determining $\langle \delta_\xi\rangle$; where $\langle \Delta u\rangle$ and $(\mathrm{d}\langle u\rangle/\mathrm{d}y)_{max}$ are approximately in phase, i.e. for $x \leqslant 0.375$ (where it is also directly out of phase with $\langle \delta_\xi\rangle$) and, to a lesser extent, for $x = 0.75$, the streamwise growth in $\langle \delta_\omega\rangle$ is more nearly consistent with a linear regime with slope approximately equal to that in steady separated flows. Especially large or small growth rates of $\langle \delta_\omega\rangle$ can be interpreted also therefore as reflecting phase differences between $\langle \Delta u\rangle$ and $(\mathrm{d}\langle u\rangle/\mathrm{d}y)_{max}$.

### 4.4. *Vorticity contours in the shear layer*

Within the thin shear-layer approximation, the velocity gradient, $\partial u/\partial y$, makes the major contribution to the vorticity in a mixing layer. Invoking this approximation, Oster & Wygnanski (1982) found evidence in phase-averaged vorticity contours during a cycle for vortex pairing events. For regions not too near to the separation point or to the downstream boundary, $\mathrm{d}\langle u\rangle/\mathrm{d}y$ should also reasonably approximate $\langle \omega\rangle$ (figure 16) in the present case as the wavelength of the flapping shear layer is much larger than the thickness of the shear layer. The growth with $x$ of the range of vertical oscillation of the shear layer is evident. The significant growth in $\langle \delta_\xi\rangle$ between $x =$

0.375 and $x = 0.5$ is striking (note that a change in contour increments is made between $x = 0.375$ and $x = 0.5$). The contours for $x \leqslant 0.5$ are quite regular, exhibiting an approximate cross-stream symmetry about the $\langle\omega\rangle$-extrema at each phase. Only a single peak, occurring during the (accelerating) phases 5 to 8, is found. In this region preceding the recirculating eddy centre (figure 6), the separated shear layer should be least affected by recirculation, and therefore should be most like the plane mixing layer. No clear evidence is found for a pairing of large-scale vortices as being the primary cause of enhanced shear-layer growth between $x = 0.375$ and $x = 0.5$. As noted above, the forcing (shedding) frequency is at least an order of magnitude smaller than the most amplified instability frequency of the shear layer, such that pairing events were not expected. The measurements were however limited in phase resolution (Oster & Wygnanski 1982 had four times the present resolution) and in streamwise spatial resolution, so that the observations do not necessarily exclude the 'collective interaction' model of Ho & Huang (1981) where the merging of many small-scale structures is postulated. Beyond $x = 0.5$, the contours become rather erratic, possibly due to increased sensitivity to errors in gradient estimation, but also due to the stronger influence of the recirculation and the wake flow. Local peaks in $\langle\omega\rangle$ are observed at $x = 0.75$, but they are fairly widely separated in phase, and should not necessarily be interpreted as indicative of large-scale vortex structures.

## 5. Summary

The shear layer separating from a front edge of a square cylinder shares features with both forced and unforced mixing layers, with steady separated flow with recirculation, as well as with forced separated boundary layers. The flow comprises a central shear layer, bounded above by an upper layer where the transition to an irrotational free stream occurs, and bounded below by a high-turbulence-intensity reverse-flow region. Phase-averaged streamlines in the cylinder reference frame indicate that the location of the centre of the recirculation eddy oscillates in the streamwise direction, with the possibility of a double centre occurring during the oscillation. The phase angle profile of the phase-averaged velocity exhibits a three-layer structure, corresponding roughly to the three different flow layers, where the phase angle is approximately constant within each layer. In an extensive region, not necessarily restricted to the shear-layer region, the phase-averaged turbulence intensity is found to be closely related in phase to the gradient of the phase-averaged velocity.

In the central shear-layer region, the phase-averaged velocity profile, when plotted in classical similarity coordinates, is well fitted for all phases and all stations by an error function profile. In the case of $\langle u'\rangle$, the collapse at various phases at the same $x$-station is adequate, but consistent deviations are found in a comparison at different $x$-stations. The growth rate, as determined by a vorticity thickness or by the similarity thickness, exhibits a somewhat step-like behaviour, unlike the linear behaviour of a classic mixing layer, but reminiscent of that of a forced mixing layer, or a separated shear layer bounding a recirculating region. The role of the recirculation region and the oscillation of the location of the eddy centre in determining shear-layer characteristics are discussed.

This work was financially supported by German Research Foundation through the Sonderforschungsbereich 210. Discussions with Dr E. Adams were helpful in the initial stages of the work. The help of Mr D. Bierwirth in setting up the experimental equipment is also acknowledged.

## REFERENCES

CANTWELL, B. & COLES, D. 1983 An experimental study of entrainment and transport in the turbulent near wake of a circular cylinder. *J. Fluid Mech.* **136**, 321–374.

CASTRO, I. P. & HAQUE, A. 1987 The structure of a turbulent shear layer bounding a separation region. *J. Fluid Mech.* **179**, 439–468.

CHERRY, N. J., HILLIER, R. & HILLIER, M. E. M. P. 1984 Unsteady measurements in a separated and reattaching flow. *J. Fluid Mech.* **144**, 13–46.

COUSTEIX, J. & HOUDEVILLE, R. 1988 Effects of unsteadiness on turbulent boundary layers. *Von Karman Inst. Lecture Series on Unsteady Aerodynamics, April 18–22, 1988.*

DJILALI, N. & GARTSHORE, I. S. 1991 Turbulent flow around a bluff rectangular plate. Part 1: Experimental Investigation. *Trans. ASME* I: *J. Fluids Engng* **113**, 51–59.

DURAO, D. F. G., HEITOR, M. V. & PEREIRA, J. C. F. 1988 Measurements of turbulent and periodic flows around a square cross-section cylinder. *Exps Fluids* **6**, 298–304.

FIEDLER, H. E. & MENSING, P. 1985 The plane turbulent shear layer with periodic excitation. *J. Fluid Mech.* **150**, 281–309.

GASTER, M., KIT, E. & WYGNANSKI, I. 1985 Large-scale structures in a forced turbulent mixing layer. *J. Fluid Mech.* **150**, 23–39.

HO, C.-H. & HUANG, L.-S. 1982 Subharmonics and vortex merging in mixing layers. *J. Fluid Mech.* **119**, 443–473.

HUSSAIN, A. K. M. F. 1986 Coherent structures and turbulence. *J. Fluid Mech.* **173**, 303–356.

HUSSAIN, A. K. M. F. & HAYAKAWA, M. 1987 Eduction of large-scale organized structures in a turbulent plane wake. *J. Fluid Mech.* **180**, 193–229.

HUSSAIN, A. K. M. F. & REYNOLDS, W. 1970 The mechanics of an organized wave in turbulent shear flow. *J. Fluid Mech.* **41**, 241–258.

KIYA, M. & SASAKI, K. 1983 Structure of a turbulent separation bubble. *J. Fluid Mech.* **137**, 83–114.

MEHTA, R. D. & WESTPHAL, R. V. 1986 Near-field turbulence properties of single- and two-stream plane mixing layers. *Exps Fluids* **4**, 257–266.

OKAJIMA, A. 1982 Strouhal numbers of rectangular cylinders. *J. Fluid Mech.* **123**, 379–398.

OSTER, D. & WYGNANSKI, I. 1982 The forced mixing layer between parallel streams. *J. Fluid Mech.* **123**, 91–130.

OWEN, F. K. & JOHNSON, D. A. 1980 Measurements of unsteady vortex flowfields. *AIAA J.* **18**, 1173–1179.

PERRY, A. E. & STEINER, T. R. 1987 Large-scale structures in turbulent wakes behind bluff bodies. Part 1. Vortex formation processes. *J. Fluid Mech.* **174**, 233–270.

RUDERICH, R. & FERNHOLZ, H. H. 1986 An experimental investigation of a turbulent flow with separation, reverse flow, and reattachment. *J. Fluid Mech.* **163**, 283–322.

SIMPSON, R. L., SHIVAPRASAD, B. G. & CHEW, Y.-T. 1983 The structure of a separating turbulent boundary layer. Part 4. Effects of periodic free-stream unsteadiness. *J. Fluid Mech.* **127**, 219–261.

WEISBROT, I. & WYGNANSKI, I. 1988 On coherent structures in a highly excited mixing layer. *J. Fluid Mech.* **195**, 137–159.